

External-field-induced transition from altermagnetic metal to fully-compensated ferrimagnetic metal in monolayer Cr_2O

San-Dong Guo^{1†}, Qiqi Luo¹, Shi-Hao Zhang², and Peng Jiang³

¹*School of Electronic Engineering, Xi'an University of Posts and Telecommunications, Xi'an 710121, China*

²*School of Physics and Electronics, Hunan University, Changsha 410082, China and*

³*Laboratory for Quantum Design of Functional Materials,
and School of Physics and Electronic Engineering,
Jiangsu Normal University, Xuzhou 221116, China*

Altermagnets and fully-compensated ferrimagnets are two canonical classes of zero-net-moment magnets. An altermagnetic (AM) half-metal cannot exist due to its AM spin splitting, while a fully-compensated ferrimagnetic (FC-FIM) metal seems impossible to realize because both spin channels remain gapless. Here, we propose that an FC-FIM metal can be realized by breaking the rotational or mirror symmetry that links two spin-opposite magnetic atoms in an AM metal. We further demonstrate that charge-carrier doping is fundamentally unable to generate a net magnetic moment in an altermagnet, whereas such a net moment can be readily induced in a fully-compensated ferrimagnet. We use the AM monolayer Cr_2O as a concrete example to validate our proposal. Either electric field or uniaxial strain can break the S_{4z} symmetry of Cr_2O , thereby inducing a transition from an AM metal to an FC-FIM metal. Uniaxial strain plus carrier doping creates a net moment in an altermagnet, and the so-called piezomagnetism is essentially a strain-driven switch from altermagnetism to fully-compensated ferrimagnetism. By analogy, we advance the concept of electromagnetism: an electric field drives the transition from altermagnetism to fully-compensated ferrimagnetism, and subsequent charge-carrier doping stabilizes a net magnetization. Our work provides a roadmap for further exploring the connection and distinction between altermagnet and fully-compensated ferrimagnet, and confirms the feasibility of FC-FIM metal.

Keywords: Fully-compensated ferrimagnetism, altermagnetism

[†]sandongyuwang@163.com

Introduction.— Emergent zero-net-magnetization magnets are attracting intense interest because they simultaneously deliver ultrahigh spintronic storage densities, robust immunity against external perturbations, and femtosecond-scale write speeds[1, 2]. From a symmetry perspective [3–6], collinear zero-net-magnetization magnets encompass three principal classes: PT -antiferromagnet (the joint symmetry (PT) of space inversion symmetry (P) and time-reversal symmetry (T)), altermagnet, and fully-compensated ferrimagnet. Although PT -antiferromagnet exhibits vanishing net magnetization, their lack of spin splitting in momentum space imposes a fundamental constraint on practical deployment. Both altermagnet and fully-compensated ferrimagnet can exhibit spin splitting without the assistance of spin-orbital coupling (SOC) in momentum space, giving rise to a variety of intriguing physical phenomena, such as the anomalous Hall and Nernst effects, non-relativistic spin-polarized currents, and the magneto-optical Kerr effects[5, 7].

The two opposite-spin sublattices of altermagnet are connected by rotational/mirror (C/M) symmetry, but the two spin sublattices in fully-compensated ferrimagnet are not connected by any symmetry[3–6, 8–11]. Experimentally, several bulk altermagnetic (AM) materials have been confirmed that exhibit momentum-dependent spin splitting[3, 7, 12–15]. Nevertheless, two-dimensional (2D) altermagnets remain a purely theoretical prediction[6, 16–27]. Fully-compensated ferri-

magnetism has traditionally been pursued in bulk systems via chemical alloying[28–30]. In 2D materials, the fully-compensated ferrimagnetic (FC-FIM) magnet can be electrostatically switched when the spin and layer are coupled with A-type antiferromagnetic (AFM) ordering[5, 6, 31–36], which has recently demonstrated in bilayer CrPS_4 under a perpendicular electric field[37]. Alternatively, the FC-FIM state can be accomplished without any lattice modification by re-engineering the spin ordering [38], or by stacking two ferromagnetic (FM) monolayers whose identical total moments exactly cancel across the heterojunction[39].

As discussed in next section, the spin-up and spin-down densities of states in altermagnets are identical, which restricts AM phases to metal or semiconductor and effectively precludes the realization of an AM half-metal. In fully-compensated ferrimagnets, the spin-up and spin-down densities of states are generally unequal, thereby permitting the existence of metallic, semiconducting, and half-metallic phases. Nevertheless, the zero-net-moment of FC-FIM is not enforced by symmetry, and in general, a gap must be maintained in at least one spin channel to guarantee compensation[5]. This constraint restricts FC-FIM phases to semiconductor or half-metal, seemingly ruling out an FC-FIM metal. However, achieving an FC-FIM metal has been proposed by electrically closing the gap of a bilayer whose interlayer coupling is AFM and whose constituent monolayer is unipolar magnetic semiconductor (UMS)[40]. Here, we demonstrate that

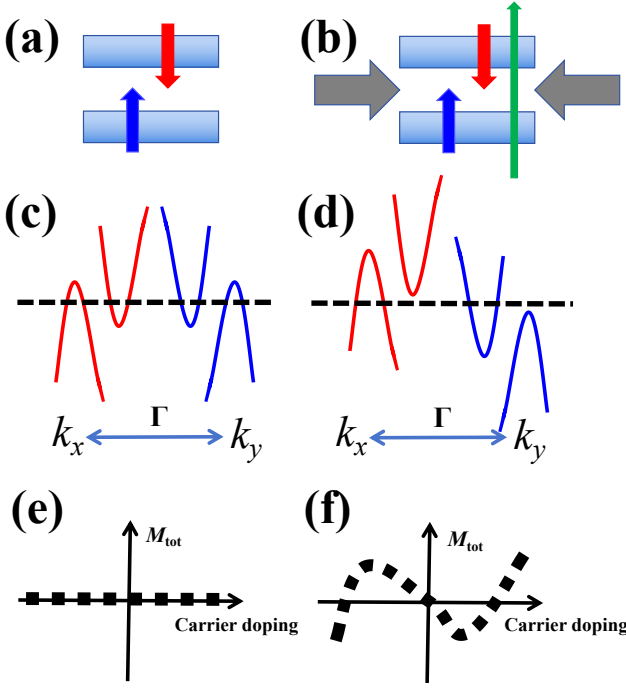


FIG. 1. (Color online) (a): the A-type AFM AM tetragonal monolayer, and the magnetic atoms with opposite spins are connected through $[C_2||S_{4z}]$ symmetry; (b): an out-of-plane electric field or in-plane uniaxial strain is applied in (a) to break $[C_2||S_{4z}]$ symmetry; (c): the (a) possesses semi-metallic bands with AM spin splitting between Γ - k_x and Γ - k_y directions; (d): the (c) transitions into an FC-FIM metallic bands due to broken $[C_2||S_{4z}]$ symmetry caused by an out-of-plane electric field or in-plane uniaxial strain; (e, f): by tuning the charge-carrier density with an electrostatic gate voltage, the AM metal (c) remains free of any net magnetic moment, whereas the FC-FIM metal (d) possesses a net moment that varies with carrier concentration. In (a, b), the blue, red, green, and horizontal gray arrows denote spin-up, spin-down, electric field, and uniaxial strain, respectively. In (c, d), the blue and red curves represent the spin-up and spin-down characteristic bands, respectively.

an FC-FIM metal can also emerge when the C/M symmetry relating spin-opposite sublattices in an AM metal is broken. We validate the scenario by first-principles calculations performed on the AM monolayer Cr_2O [41].

Proposal.— An FC-FIM metal can be obtained by breaking the C/M symmetry that connects spin-opposite magnetic atoms in an AM metal. Here we illustrate our proposal with an A-type AFM tetragonal AM semimetal (Figure 1 (a)). The magnetic atoms with opposite spins are connected through $[C_2||S_{4z}]$ symmetry (with S_{4z} being a roto-inversion operation), showing AM spin-splitting between Γ - k_x and Γ - k_y directions (Figure 1 (c)) with d -wave symmetry. When an out-of-plane electric field (Here, the external electric field can also be equivalently realized through the substrate or a ferroelectric heterojunction.) or in-plane uniaxial strain is applied (Figure 1 (b)), the $[C_2||S_{4z}]$ symmetry is broken, and the

system becomes an FC-FIM metal, showing global spin-splitting (Figure 1 (d)) with s -wave symmetry.

For altermagnets, the spin-up and spin-down energy bands exhibit the following relationship:

$$E_{\uparrow}(\vec{k}) = [C_2 || O]E_{\uparrow}(\vec{k}) = E_{\downarrow}(O\vec{k}) \quad (1)$$

where O denotes C/M symmetry. For the high-symmetry point Γ , we have $O\Gamma=\Gamma$, and then $E_{\uparrow}(\Gamma)=E_{\downarrow}(\Gamma)$. However, for a fully-compensated ferrimagnet, $E_{\uparrow}(\Gamma)\neq E_{\downarrow}(\Gamma)$ in general.

For altermagnets, according to Equation 1, we obtain:

$$g_{\uparrow}(E) = \sum_{\vec{k}} \delta[E - E_{\uparrow}(\vec{k})] = \sum_{\vec{k}} \delta[E - E_{\downarrow}(O\vec{k})] \quad (2)$$

When \vec{k} spans the entire first Brillouin zone (BZ), $O\vec{k}$ also spans the entire BZ. Therefore, Equation 2 can be rewritten as:

$$\sum_{\vec{k}} \delta[E - E_{\downarrow}(O\vec{k})] = \sum_{\vec{k}'} \delta[E - E_{\downarrow}(\vec{k}')] = g_{\downarrow}(E) \quad (3)$$

where $g_{\uparrow}(E)$ and $g_{\downarrow}(E)$ denote spin-up and spin-down density of states. According to Equation 2 and Equation 3, $g_{\uparrow}(E)$ and $g_{\downarrow}(E)$ are identical ($g_{\uparrow}(E)=g_{\downarrow}(E)$) in altermagnets, but they are generally not equal ($g_{\uparrow}(E)\neq g_{\downarrow}(E)$) in fully-compensated ferrimagnets.

In general, the net magnetization M_{tot} in the magnet can be written as:

$$M_{tot} = \mu_B \int_{-\infty}^{E_F} (g_{\uparrow}(E) - g_{\downarrow}(E))dE \quad (4)$$

where μ_B is the Bohr magneton, E_F is the Fermi level. For both altermagnets and fully-compensated ferrimagnets, M_{tot} is equal to zero. Nevertheless, when shifting the Fermi level E_F to vary the charge-carrier concentration, M_{tot} remains exactly zero in altermagnets (Figure 1 (e)) due to $g_{\uparrow}(E)=g_{\downarrow}(E)$ (In carrier doping, the magnetic ground state is assumed to remain unchanged.), whereas it is generally non-zero in fully-compensated ferrimagnets (Figure 1 (f)) due to $g_{\uparrow}(E)\neq g_{\downarrow}(E)$. Below, we use the AM Cr_2O monolayer as an example to validate our proposal.

Computational detail.— The spin-polarized first-principles calculations are carried out within density functional theory (DFT)[42, 43] and the projector augmented-wave (PAW) method by using the Vienna Ab Initio Simulation Package (VASP)[44–46]. We use the Perdew-Burke-Ernzerhof generalized gradient approximation (GGA)[47] as the exchange-correlation functional. We add Hubbard correction $U=2$ eV[41] for d -orbitals of Cr atoms within the rotationally invariant approach proposed by Dudarev et al[48]. The kinetic energy cutoff of 550 eV, total energy convergence criterion of 10^{-8} eV, and force convergence criterion of 0.001 eVÅ⁻¹ are adopted to obtain accurate results. A vacuum

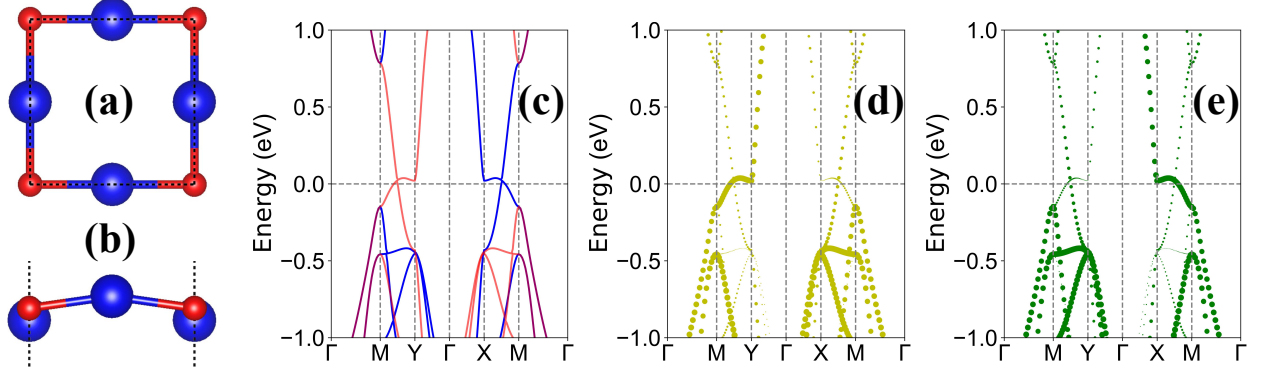


FIG. 2. (Color online) For Cr_2O , (a, b): the top and side views of the crystal structures; (c): the spin-polarized band structures; (d, e): the upper- and lower-layer Cr projected band structures. In (a, b), the large blue and small red spheres represent Cr and O atoms, respectively. In (c), the blue and red curves denote the spin-up and spin-down characteristic bands, respectively, while the purple indicates the spin-degenerate bands. In (d, e), the size of the circles is proportional to the atomic weight.

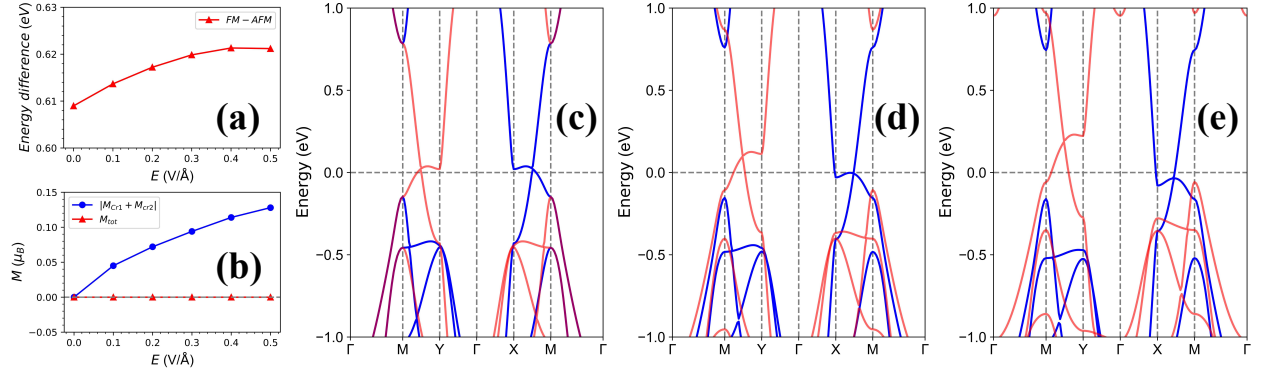


FIG. 3. (Color online) For Cr_2O , (a): the energy difference between FM and AFM orderings as a function of electric field E ; (b): the absolute value of the sum of the magnetic moments of the upper- and lower-layer Cr atoms ($|M_{\text{Cr}1} + M_{\text{Cr}2}|$), along with the total magnetic moment (M_{tot}), as a function of electric field E ; (c, d, e): the spin-polarized band structures at representative $E = +0.00, +0.20$ and $+0.40$ V/Å. In (c, d, e), the blue and red curves denote the spin-up and spin-down characteristic bands, respectively, while the purple indicates the spin-degenerate bands.

layer exceeding 16 Å along the z -direction is employed to eliminate spurious interactions between periodic images. The BZ is sampled with a $14 \times 14 \times 1$ Monkhorst-Pack k -point meshes for both structural relaxation and electronic structure calculations. The crystal structure and atomic-position optimizations are also carried out using GGA+ U . In the calculations under an applied electric field, the atomic positions are optimized as well.

Material realization.— Monolayer Cr_2O has been theoretically predicted to be an AM metal with excellent stability, and it can be exfoliated from bulk CrO along the $[001]$ direction[41]. Its crystal structures are plotted in Figure 2 (a, b), which is composed of three monatomic planes in the sequence Cr-O-Cr and crystallizes in the $P4m2$ space group (No.115). The A-type AFM state of Cr_2O is the most stable magnetic configuration as the AM magnetic ordering. The optimized equilibrium lattice constants are $a=b=3.91$ Å within GGA+ U .

The spin-polarized band structure of Cr_2O , along with

the projected bands for the upper- and lower-layer Cr atoms, are shown in Figure 2 (c, d, e). It is clearly seen that Cr_2O is an AM semimetal, exhibiting d -wave symmetric spin splitting due to $[C_2||S_{4z}]$ symmetry. These provide the essential basis for transforming Cr_2O into an FC-FIM metal via electric field or uniaxial strain tuning. According to Figure 2 (d, e), the bands of two high-symmetry paths connected by C_{4z} symmetry exhibit clearly distinct weights of the upper and lower Cr atoms, offering favorable conditions for band-structure tuning via an electric field.

First, we consider the modulation of Cr_2O by an electric field. An electric field can generate a layer-dependent electrostatic potential, rendering the upper and lower Cr atoms inequivalent and further breaking the S_{4z} symmetry[6, 49]. Viewed in reciprocal space, the field shifts the bands that carry distinct upper- and lower-layer Cr weights relative to each other, inducing new electronic states. The energy difference between FM

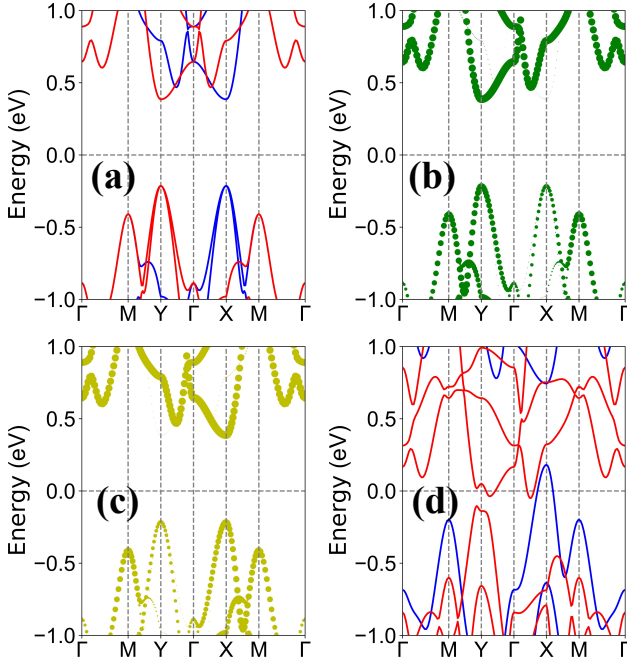


FIG. 4. (Color online) For $\text{Mg}(\text{CoN})_2$, (a): the spin-polarized band structures without electric field; (b, c): the upper- and lower-layer Co projected band structures without electric field; (d): the spin-polarized band structures at $E = +0.25$ V/Å. In (a, d), the blue and red curves denote the spin-up and spin-down characteristic bands, respectively, while the purple indicates the spin-degenerate bands. In (b, c), the size of the circles is proportional to the atomic weight.

and AFM orderings as a function of electric field E are plotted in Figure 3 (a). Within the range of electric field considered, the AFM ordering remains the ground state, ensuring that Cr_2O retains its altermagnetism. The absolute value ($|M_{\text{Cr}1} + M_{\text{Cr}2}|$) of the sum of the magnetic moments of the upper- and lower-layer Cr atoms along with the total magnetic moment as a function of electric field E are plotted in Figure 3 (b). It is clear that the total magnetic moment of Cr_2O remains zero within considered E range, satisfying the zero-net-moment requirement of a fully-compensated ferrimagnet[5]. As the E is applied, the $|M_{\text{Cr}1} + M_{\text{Cr}2}|$ deviates from zero and gradually increases, which from another perspective indicates the emergence of fully-compensated ferrimagnetism.

The spin-polarized band structures at representative $E = +0.00$, $+0.20$ and $+0.40$ V/Å are plotted in Figure 3 (c, d, e). Under an applied electric field, Cr_2O remains metallic, but the bands of two high-symmetry paths connected by C_{4z} symmetry exhibit pronounced asymmetry, and the spin degeneracy along the Γ -M path is lifted. In other words, the spin-splitting symmetry of Cr_2O switches from d -wave to s -wave character. Upon reversal of the electric field direction, the corresponding change of the bands of two high-symmetry paths connected by C_{4z} symmetry is also reversed (see FIG.S1[50]).

The Cr_2O exhibits zero-net magnetic moment, metallicity, and s -wave spin splitting under an applied electric field, enabling it to transform into an FC-FIM metal.

According to our recent proposal[40], if one layer of a bilayer system with AFM interlayer coupling is a UMS, the system's band gap can be closed by an electric field and realize an FC-FIM metal. This strategy can also be applied to A-type AFM AM monolayer. If the projected band structure of one magnetic-atom layer exhibits unipolar character, its gap can likewise be closed by an electric field, yielding an FC-FIM metal. We take monolayer $\text{Mg}(\text{CoN})_2$ [49] as an example to validate our proposal. Monolayer $\text{Mg}(\text{CoN})_2$ has been confirmed to be an A-type AFM AM semiconductor, and its crystal structure is shown in FIG.S2[50] with the $P4m2$ space group (No.115). The spin-polarized band structure of $\text{Mg}(\text{CoN})_2$, along with the projected bands for the upper- and lower-layer Co atoms, are shown in Figure 4 (a, b, c). By comparing Figure 4 (a) with Figure 4 (b) or Figure 4 (a) with Figure 4 (c), it can be inferred that the projected band structure of one Co layer exhibits unipolar character (Near the valence band maximum (VBM) and conduction band minimum (CBM), the bands are dominated by the same spin character.), which provides the essential condition for realizing an FC-FIM metal through electric-field control[40]. When an electric field of $E = +0.25$ V/Å is applied, the total magnetic moment of $\text{Mg}(\text{CoN})_2$ is zero, its band structure exhibits metallic character and spin splitting (see Figure 4 (d)), and then it indeed turns into an FC-FIM metal.

Next, we discuss the effect of uniaxial strain on the electronic structure of Cr_2O . We use a/a_0 to simulate uniaxial strain along the x -direction, and the $a/a_0 < 1$ ($a/a_0 > 1$) means the compressive (tensile) strain, where a and a_0 are the strained and unstrained lattice constants. Uniaxial strain directly alters the crystal structure, thereby breaking the S_{4z} symmetry of Cr_2O . Analogous strain engineering has been applied to other AM semiconductors to induce valley polarization[19–23]. The a/a_0 dependence of the energy difference between FM and AFM orderings is displayed in Figure 5(a). Throughout the examined range, the AFM phase stays lower in energy, so Cr_2O preserves AM ground state. Figure 5(b) shows the absolute value ($|M_{\text{Cr}1} + M_{\text{Cr}2}|$) of the sum of the magnetic moments on the upper- and lower-layer Co atoms, together with the total magnetic moment, as a function of a/a_0 . The total magnetic moment remains exactly zero, satisfying the fully-compensated ferrimagnetic requirement, whereas $|M_{\text{Cr}1} + M_{\text{Cr}2}|$ progressively departs from zero under increasing both compressive and tensile strain, providing direct evidence for the strain-induced emergence of fully-compensated ferrimagnetism[5].

The spin-polarized band structures at representative $a/a_0 = 0.96$, 0.00 and 1.04 are shown in Figure 5 (c, d, e). Upon applying strain, Cr_2O retains its metallic char-

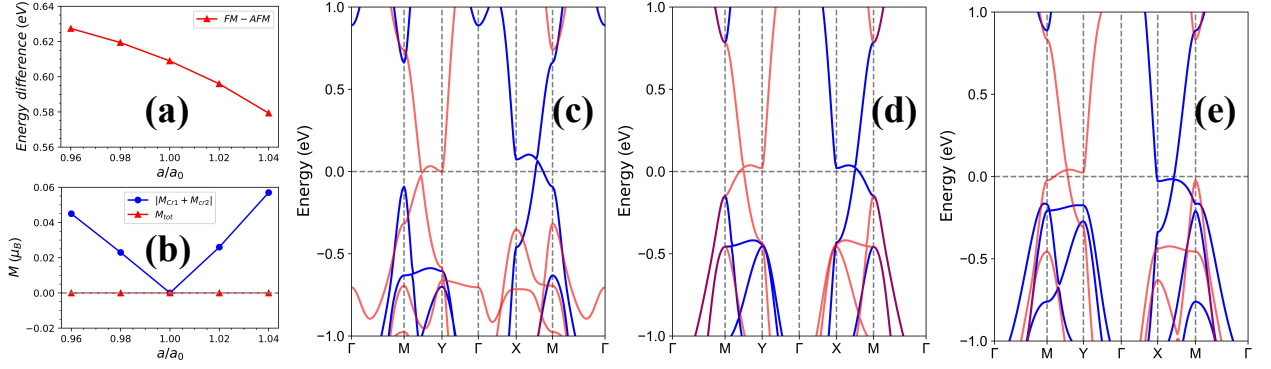


FIG. 5. (Color online) For Cr_2O , (a): the energy difference between FM and AFM orderings as a function of uniaxial strain a/a_0 ; (b): the absolute value of the sum of the magnetic moments of the upper- and lower-layer Cr atoms ($|M_{\text{Cr}1} + M_{\text{Cr}2}|$), along with the total magnetic moment (M_{tot}), as a function of uniaxial strain a/a_0 ; (c, d, e): the spin-polarized band structures at representative $a/a_0=0.96, 1.00$ and 1.04 . In (c, d, e), the blue and red curves denote the spin-up and spin-down characteristic bands, respectively, while the purple indicates the spin-degenerate bands.

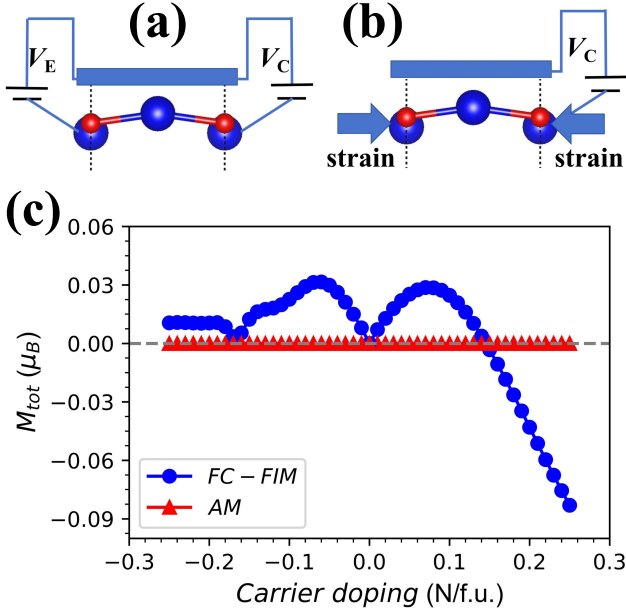


FIG. 6. (Color online) For Cr_2O , (a): by using dual-gate technology, the electric field E with V_E and the charge-carrier density N with V_C can be tuned independently, and the Cr_2O can be turned into a fully-compensated ferrimagnet, exhibiting a net magnetic moment; (b): The V_E in (a) can be replaced by uniaxial strain to achieve fully-compensated ferrimagnetism, and generate a net magnetic moment; (c): the total magnetic moment as a function of carrier concentration for the unstrained case (AM) and for $a/a_0=1.04$ (FC-FIM).

acter; however, the bands along the two high-symmetry paths related by C_{4z} symmetry show a marked asymmetry, and the spin degeneracy along the Γ -M path is removed. Consequently, the spin-splitting symmetry of Cr_2O transitions from a d -wave to an s -wave character. It is also found that the band modifications induced by tensile-to-compressive strain mirror those pro-

duced by reversing the electric field direction. If uniaxial strain is applied along the y -direction, similar results are obtained, and the sole difference is that the bands on the two paths linked by C_{4z} symmetry are interchanged. Subject to strain, Cr_2O retains metallicity and zero-net magnetic moment, while developing s -wave spin splitting, enabling its transition into an FC-FIM metal.

Finally, we examine how charge-carrier doping affects the total magnetic moment of Cr_2O . In 2D AM semiconductor, the emergence of a net magnetic moment under the cooperative action of uniaxial strain and charge-carrier doping is designated as piezomagnetism[19]. Here, we emphasize that the underlying origin of this effect is the strain-induced transition from an AM to an FC-FIM state under uniaxial deformation (According to Figure 1 (e, f), only fully-compensated ferrimagnets can produce a net magnetic moment upon charge-carrier doping.). Under biaxial strain, the system remains AM phase and no piezomagnetic response emerges. Analogously, we can also introduce an electromagnetic counterpart: by driving an altermagnet (more generally, including PT -antiferromagnet) into a fully-compensated ferrimagnet with an electric field, subsequent charge-carrier doping can produce a net magnetic moment. This electrically controlled magnetoelectric phenomenon is designated electromagnetism.

Dual-gating technology has been implemented in graphene to enable tunable control of proton transport and hydrogenation[51]. Dual-gating by applying electrostatic gate potentials to both surfaces of a 2D system enables independent control of the electric field E and the charge-carrier density N (see Figure 6 (a)), and the electromagnetism can be realized in Cr_2O . The piezomagnetism in Cr_2O can also be achieved through the combined application of uniaxial strain and single-gate electrostatic control (see Figure 6 (b)). Owing to computational constraints, the simultaneous imposition of an

external electric field and charge-carrier doping cannot be implemented within the VASP code. Herein, we exclusively impose uniaxial strain together with charge-carrier doping to verify the emergence of a net magnetic moment in Cr_2O .

The total magnetic moment as a function of carrier concentration for the unstrained case and for $a/a_0=1.04$ are plotted in Figure 6 (c). It is evident that, in the absence of strain, Cr_2O remains an altermagnet exhibiting no net magnetic moment, whereas under applied strain it transitions to a fully-compensated ferrimagnet, thereby generating a finite net magnetic moment. Across the entire doping window investigated under finite strain, the AFM ordering of Cr_2O persists as the ground state, retaining its FC-FIM character (see FIG.S3[50]). To unambiguously demonstrate that a fully-compensated ferrimagnet can host a net magnetic moment under charge-carrier doping, we select the prototypical FC-FIM semiconductor CrMoC_2S_6 [52, 53] and Cr_2CHCl [54, 55] for further validation of this effect. Their band structures, the energy difference between FM and AFM states as a function of doping concentration, and the total magnetic moment as a functions of doping concentration are presented in FIG.S4, FIG.S5 and FIG.S6[50]. It is evident that charge-carrier doping can induce a net magnetic moment in FC-FIM semiconductor CrMoC_2S_6 and Cr_2CHCl .

Discussion and conclusion.— A key band-structure distinction between altermagnet and fully-compensated ferrimagnet is that in the former every band at the high-symmetry Γ point remains spin-degenerate, whereas in the latter this need not be the case. Moreover, gate-controlled charge-carrier doping leaves an altermagnet with zero-net-moment, whereas the same procedure generates a finite magnetization in a fully-compensated ferrimagnet. For practical use, an FC-FIM semiconductor must be charge-carrier-doped, which will generate a net magnetic moment. In contrast, FC-FIM half-metal or metal already possesses intrinsic carriers and can therefore retain zero-net-moment. Finally, we point out that either thermal excitation or light-induced carrier injection can also give rise to a net magnetization in a fully-compensated ferrimagnet.

In summary, we demonstrate that breaking the C/M symmetry which couples spin-opposite magnetic atoms in an AM metal provides a direct route to realizing an FC-FIM metal. First-principles calculations show that AM Cr_2O can form an FC-FIM metal via electric field or uniaxial strain. By analogy with piezomagnetism, we introduce the concept of electromagnetism. We further point out that the net magnetic moment induced by combined strain or electric field with carrier doping essentially arises from the external-field-driven transition of the system from the AM state to the FC-FIM state. Our work provides a feasible strategy for realizing FC-FIM metal, along with the connection and distinction between

the AM and FC-FIM states.

This work is supported by Natural Science Basis Research Plan in Shaanxi Province of China (2025JC-YBMS-008) We are grateful to Shanxi Supercomputing Center of China, and the calculations were performed on TianHe-2.

-
- [1] X. Hu, Half-metallic antiferromagnet as a prospective material for spintronics, *Adv. Mater.* **24**, 294 (2012).
 - [2] T. Jungwirth, J. Sinova, A. Manchon, X. Marti, J. Wunderlich and C. Felser, The multiple directions of antiferromagnetic spintronics, *Nat. Phys.* **14**, 200 (2018).
 - [3] L. Šmejkal, J. Sinova and T. Jungwirth, Beyond conventional ferromagnetism and antiferromagnetism: A phase with nonrelativistic spin and crystal rotation symmetry, *Phys. Rev. X* **12**, 031042 (2022).
 - [4] I. Mazin, Altermagnetism—a new punch line of fundamental magnetism, *Phys. Rev. X* **12**, 040002 (2022).
 - [5] Y. Liu, S. D. Guo, Y. Li and C. C. Liu, Two-dimensional fully-compensated Ferrimagnetism, *Phys. Rev. Lett.* **134**, 116703 (2025).
 - [6] S. D. Guo, Valley polarization in two-dimensional zero-net-magnetization magnets, *Appl. Phys. Lett.* **126**, 080502 (2025).
 - [7] L. Bai, W. Feng, S. Liu, L. Šmejkal, Y. Mokrousov, and Y. Yao, Altermagnetism: Exploring New Frontiers in Magnetism and Spintronics, *Adv. Funct. Mater.* **34**, 2409327 (2024).
 - [8] T. Kawamura, Kazuyoshi Yoshimi, Kenichiro Hashimoto, Akito Kobayashi and Takahiro Misawa, Compensated Ferrimagnets with Colossal Spin Splitting in Organic Compounds, *Phys. Rev. Lett.* **132**, 156502 (2024).
 - [9] M. Žić, K. Rode, N. Thiagarajah, Y. C. Lau, D. Betto, J. M. D. Coey, S. Sanvito, K. J. O’Shea and C. A. Ferguson, Designing a fully compensated half-metallic ferrimagnet, *Phys. Rev. B* **93**, 140202(R) (2016).
 - [10] H. A. Zhou, T. Xu, H. Bai and W. Jiang, Efficient Spintronics with Fully Compensated Ferrimagnets, *J. Phys. Soc. Jpn.* **90**, 081006 (2021).
 - [11] I. Galanakis and E. Sasoğlu, High T_C half-metallic fully-compensated ferrimagnetic Heusler compounds, *Appl. Phys. Lett.* **99**, 052509 (2011).
 - [12] Z. Zhou, X. Cheng, M. Hu et al., Manipulation of the altermagnetic order in CrSb via crystal symmetry, *Nature* **638**, 645 (2025).
 - [13] J. Ding, Z. Jiang, X. Chen et al., Large Band Splitting in g -Wave Altermagnet CrSb , *Phys. Rev. Lett.* **133**, 206401 (2024).
 - [14] B. Jiang, M. Hu, J. Bai et al., A metallic room-temperature d-wave altermagnet. *Nat. Phys.* **21**, 754 (2025).
 - [15] F. Zhang X. Cheng, Z. Yin et al., Crystal-symmetry-paired spinvalley locking in a layered room-temperature metallic altermagnet candidate, *Nature Phys.* **21**, 760 (2025).
 - [16] S. D. Guo, X. S. Guo and G. Wang, Valley polarization in two-dimensional tetragonal altermagnetism, *Phys. Rev. B* **110**, 184408 (2024).
 - [17] Y. Liu, J. Yu and C. C. Liu, Twisted Magnetic Van der

- Waals Bilayers: An Ideal Platform for Altermagnetism, *Phys. Rev. Lett.* **133**, 206702 (2024).
- [18] H.-Y. Ma, M. L. Hu, N. N. Li, J. P. Liu, W. Yao, J. F. Jia and J. W. Liu, Multifunctional antiferromagnetic materials with giant piezomagnetism and noncollinear spin current, *Nat. Commun.* **12**, 2846 (2021).
- [19] H.-Y. Ma, M. L. Hu, N. N. Li, J. P. Liu, W. Yao, J. F. Jia and J. W. Liu, Multifunctional antiferromagnetic materials with giant piezomagnetism and noncollinear spin current, *Nat. Commun.* **12**, 2846 (2021).
- [20] S.-D. Guo, X.-S. Guo, K. Cheng, K. Wang, and Y. S. Ang, Piezoelectric altermagnetism and spin-valley polarization in Janus monolayer Cr_2SO , *Appl. Phys. Lett.* **123**, 082401 (2023).
- [21] X. Chen, D. Wang, L. Y. Li and B. Sanyal, Giant spin-splitting and tunable spin-momentum locked transport in room temperature collinear antiferromagnetic semimetallic CrO monolayer, *Appl. Phys. Lett.* **123**, 022402 (2023).
- [22] Y. Zhu, T. Chen, Y. Li, L. Qiao, X. Ma, C. Liu, T. Hu, H. Gao and W. Ren, Multipiezo Effect in Altermagnetic V_2SeTeO Monolayer, *Nano Lett.* **24**, 472 (2024).
- [23] Y. Wu, L. Deng, X. Yin, J. Tong, F. Tian and X. Zhang, Valley-Related Multipiezo Effect and Noncollinear Spin Current in an Altermagnet $\text{Fe}_2\text{Se}_2\text{O}$ Monolayer, *Nano Lett.* **24**, 10534 (2024).
- [24] S. D. Guo, Hidden altermagnetism, *Front. Phys.* **21**, 025201 (2026).
- [25] J. Sodequist and T. Olsen, Two-dimensional altermagnets from high throughput computational screening: Symmetry requirements, chiral magnons, and spin-orbit effects, *Appl. Phys. Lett.* **124**, 182409 (2024).
- [26] S. Zeng and Y. J. Zhao, Description of two-dimensional altermagnetism: Categorization using spin group theory, *Phys. Rev. B* **110**, 054406 (2024).
- [27] S. D. Guo and G. Wang, External-field-induced altermagnetism in experimentally synthesized monolayer CrX_3 ($\text{X}=\text{Cl}, \text{Br}$ and I), *Appl. Phys. Lett.* **127**, 042402 (2025).
- [28] H. van Leuken and R. A. de Groot, Half-Metallic Antiferromagnets, *Phys. Rev. Lett.* **74**, 1171 (1995).
- [29] H. Akai and M. Ogura, Half-Metallic Diluted Antiferromagnetic Semiconductors, *Phys. Rev. Lett.* **97**, 026401 (2006).
- [30] S. Wurmehl, H. C. Kandpal, G. H. Fecher, and C. Felser, Valence electron rules for prediction of half-metallic compensated-ferrimagnetic behaviour of Heusler compounds with complete spin polarization, *J. Phys.: Condens. Matter* **18**, 6171 (2006).
- [31] S. D. Guo, Y. L. Tao, Z. Y. Zhuo, G. Zhu and Y. S. Ang, Electric-field-tuned anomalous valley Hall effect in A-type hexagonal antiferromagnetic monolayers, *Phys. Rev. B* **109**, 134402 (2024).
- [32] S. D. Guo, W. Xu, Y. Xue, G. Zhu and Y. S. Ang, Layer-locked anomalous valley Hall effect in a two-dimensional A-type tetragonal antiferromagnetic insulator, *Phys. Rev. B* **109**, 134426 (2024).
- [33] S. D. Guo, P. Li and G. Wang, First-principles calculations study of valley polarization in antiferromagnetic bilayer systems, *Phys. Rev. B* **111**, L140404 (2025).
- [34] L. Zhang, S. D. Guo and G. Wang, Spontaneous and reversible spin-splitting in ferroelectric A-type antiferromagnetism, *J. Mater. Chem. C* **12**, 8485 (2024).
- [35] J. Feng, X. Zhou, J. Chen, M. Xu, X. Yang and Y. Li, Ferroelectric antiferromagnetic lifting of spin-valley degeneracy, *Phys. Rev. B* **111**, 214446 (2025).
- [36] N. Cheng, H. Cheng, X. Zhao, G. Hu, X. Yuan and J. Ren, Ferroelectric polarization manipulates the layer-polarized anomalous Hall effect in bilayers with fully compensated ferrimagnetism, *Phys. Rev. B* **111**, 195154 (2025).
- [37] F. Yao, M. Liao, M. Gibertini et al., Switching on and off the spin polarization of the conduction band in antiferromagnetic bilayer transistors, *Nat. Nanotechnol.* **20**, 609 (2025).
- [38] S. D. Guo, S. Chen and G. Wang, Spin ordering induced fully compensated ferrimagnetism achieved in bilayers of $\text{Cr}_2\text{C}_2\text{S}_6$, *Phys. Rev. B* **112**, 134430 (2025).
- [39] S. D. Guo, J. He and Y. S. Ang, Achieving fully-compensated ferrimagnetism through two-dimensional $\text{CrI}_3/\text{CrGeTe}_3$ heterojunctions, *Appl. Phys. Lett.* in press (2025).
- [40] S. D. Guo, R. Bian, F.-R. Fan and A. Stroppa, A route to fully-compensated ferrimagnetic metal: electric-field annihilation of the bilayer bandgap, <https://doi.org/10.48550/arXiv.2508.08609> (2025).
- [41] X. Zhang, P. Jiang, L.-Y. Xu, L. Wang, L. Liu, H.-M. Huang, T. Cao and Y.-L. Li, Giant Spin Splitting and Anisotropic Spin Polarization in 2D Altermagnet Cr_2O , *Nano Lett.* **25**, 16547 (2025).
- [42] P. Hohenberg and W. Kohn, Inhomogeneous Electron Gas, *Phys. Rev.* **136**, B864 (1964).
- [43] W. Kohn and L. J. Sham, Self-Consistent Equations Including Exchange and Correlation Effects, *Phys. Rev.* **140**, A1133 (1965).
- [44] G. Kresse, Ab initio molecular dynamics for liquid metals, *J. Non-Cryst. Solids* **193**, 222 (1995).
- [45] G. Kresse and J. Furthmüller, Efficiency of ab-initio total energy calculations for metals and semiconductors using a plane-wave basis set, *Comput. Mater. Sci.* **6**, 15 (1996).
- [46] G. Kresse and D. Joubert, From ultrasoft pseudopotentials to the projector augmented-wave method, *Phys. Rev. B* **59**, 1758 (1999).
- [47] J. P. Perdew, K. Burke and M. Ernzerhof, Generalized gradient approximation made simple, *Phys. Rev. Lett.* **77**, 3865 (1996).
- [48] S. L. Dudarev, G. A. Botton, S. Y. Savrasov, C. J. Humphreys, and A. P. Sutton, Electron-energy-loss spectra and the structural stability of nickel oxide: An LSDA+U study, *Phys. Rev. B* **57**, 1505 (1998).
- [49] R. W. Zhang, C. X. Cui, R. Z. Li, J. Y. Duan, L. Li, Z. M. Yu and Y. G. Yao, Predictable gate-field control of spin in altermagnets with spin-layer coupling, *Phys. Rev. Lett.* **133**, 056401 (2024).
- [50] See Supplemental Material at [] for the the related energy band structures; the crystal structures, the energy differences between FM and AFM orderings as a function of carrier concentration and the total magnetic moments as a function of carrier concentration.
- [51] J. Tong, Y. Fu, D. Domaretskiy et al., Control of proton transport and hydrogenation in double-gated graphene, *Nature* **630**, 619 (2024).
- [52] S. D. Guo, X. S. Guo, D. C. Liang and G. Wang, Symmetry-breaking induced transition among net-zero-magnetization magnets, *J. Mater. Chem. C* **13**, 11997 (2025).
- [53] P. Wang, D. X. Wu, K. Zhang and X. J. Wu, Two-Dimensional Quaternary Transition Metal Sulfide CrMoA_2S_6 ($\text{A}=\text{C}, \text{Si}, \text{or Ge}$): A Bipolar Antiferromagnetic Semiconductor with a High Néel Temperature, *J.*

- Phys. Chem. Lett. **13**, 3850 (2022).
- [54] C. Si, J. Zhou, and Z. Sun, Half-Metallic Ferromagnetism and Surface Functionalization-Induced Metal-Insulator Transition in Graphene-like Two-Dimensional Cr_2C Crystals, ACS Appl. Mater. Interfaces **7**, 17510 (2015).
- [55] D.-C. Liang, S. D. Guo and S. Chen, Anomalous valley Hall effect in electric-potential difference antiferromagnetic Cr_2CHCl monolayer, Appl. Phys. Lett. **125**, 242402 (2024).